Archives of Civil and Mechanical Engineering (2022) 22:109
https://doi.org/10.1007/s43452-022-00427-3

ORIGINAL ARTICLE

Influence of metallic grid and fiber reinforced concrete strengthening on the shielding and impact resistance of concrete walls

Tian-Feng Yuan[1] · Jin-Seok Choi[1] · Young-Hwi Kim[2] · Young-Soo Yoon[1]

Received: 21 October 2021 / Revised: 13 March 2022 / Accepted: 19 March 2022

Abstract
In modern society, an ever-increasing emphasis is placed on structural safety design that not only considers external loading but extends to reduced electromagnetic interference. Generally, studies only consider shielding effectiveness of strengthening method or materials, and few studies have considered the relationship between damaged areas and shielding effectiveness. Therefore, the influence of metallic grid parameters and fiber reinforced concrete (HSDC) on shielding effectiveness with and without impact loading are studied in this research. Concrete wall strengthening with four types of metallic grid and three thickness types of HSDC were considered. Moreover, the relationship between damaged area ratio and shielding effectiveness was evaluated utilizing the low-velocity drop-weight impact test. In specimens with metallic grid or HSDC, shielding effectiveness with strengthening layer (13.4–64.1%) or thickness (35.6–46.2%) increase and grid size (> 7.8%) decreased. Specimen strengthened by smaller than 55.1% and 101% of the free space area ratio of single and double layer, respectively, exhibit more than 40 dB shielding effectiveness. For the specimen strengthened with HSDC, shielding effectiveness increased with strengthening area, except smaller than 6%. The smallest metallic grid and the thickest HSDC strengthening specimen exhibited improved impact resistance and great shielding effectiveness after impact loading.

Keywords Metallic grid · High-strength high ductility concrete · Electromagnetic shielding · Impact resistance · Damage area ratio · Strengthening

1 Introduction

With the sustained development of the national economy many high-rise, commercial and civil buildings have emerged, as well as the increasing need for electrical power. People are also more and more concerned about the surrounding electromagnetic environment with the improving living conditions. Electromagnetic interference (EMI) pollution has been recognized as a worrying danger for commercial apparatus [1, 2], biological systems (human health) [2, 3], high-quality information [4] and defense safe technology [1, 2, 5, 6]. Therefore, this pollution has become an extremely serious universal problem, and it has renewed focus to carry out extensive research into EMI shielding materials and methods [2, 5, 6]. The EMI shielding materials and methods are primarily focused on the reflection and /or absorption of EMI radiation to prevent the radiation penetration passing through the shielding materials and methods. In general, conductive materials (such as metals, carbon materials, magnetic materials) are extensively used for EMI shielding according to their high reflectivity. Hence, the protection of a special environment is nowadays procured using a shielding enclosure made of metallic walls. However, despite its effectiveness in shielding from EMI, it is considered heavy and hard to be installed over existing buildings or walls.

Therefore, the application of cementitious composites containing conductive materials signals an effective

✉ Young-Soo Yoon
ysyoon@korea.ac.kr

Tian-Feng Yuan
yuantianfeng@korea.ac.kr

Jin-Seok Choi
radiance@korea.ac.kr

Young-Hwi Kim
younghwi.kim@autodesk.com

1 School of Civil, Environmental and Architectural Engineering, Korea University, 125 Anam-ro, Seongbuk-gu, Seoul 02841, Republic of Korea

2 COO-WWS APAC Technical Sales Korea, Autodesk, Seoul 06164, Republic of Korea

Published online: 05 April 2022

alternative to metallic shielded enclosure since it can be used during construction (fabrication walls) and/or to readily plaster existing walls without the adopting of any special adhesive [1, 7]. Some tentative research has been completed using conductive materials inside the cementitious composites. Typically, mixing an adequate amount of a conductive materials, such as metallic fiber, into cementitious composites during the mixing stage can improve the SE of composites, resulting in the formation of an electrical network within the composite matrix. The mechanical properties of fiber reinforced concrete are improved as the fiber content is increased within an appropriate content range. In this case, electrical networks form within the composite matrix are further influenced, and the percolation threshold should be considered. Through much research [2, 5, 8, 9], the percolation threshold depends on factors such as the shape, morphology, aspect ratio, distribution, and concentration of the metallic fibers. The SE properties of the cementitious composites remained constant or decreased when over the percolation threshold. As proven in previous research [1, 5, 6], the SE of fiber reinforced cementitious composites presented as almost unchanged after a certain amount of metallic fiber volume fraction. Similarly, this phenomenon also applies to the metallic powder added in cementitious composites. Therefore, conductive materials (such as iron ingredient materials [2, 10], steel furnace slag [5, 11–13], metal oxides [2, 13], and conducting polymers [14–16]) are not the more the better, but one can most desirable to the certain volume fraction.

In recent years, the progress of nanotechnologies has increased the use of nanostructured materials as strengthening in conventional cementitious composites in many fields of research, exhibiting some effective shielding properties. Though the nanostructured materials combined with cementitious composites have many advantages, they tolerate a lack of economy and processability (such as workability and dispersibility) during large-scale production of cementitious composites. Carbonaceous nanomaterial (graphite/expanded graphite, graphene, and carbon nanotubes) have been widely used in cementitious composites and investigated for EMI SE properties [2, 3, 15, 17–19]. However, the large surface area of carbonaceous nanomaterials increased many properties, the main impedance to using carbonaceous nanomaterials in cementitious composites is the necessary to a large weight ratio (or volume ratio), which deteriorates the mechanical properties. A great deal of study is still necessary for the evaluation of such cementitious composites in the cause of their SE properties. However, most importantly, a lot of effort has been made in this direction; unfortunately, most evaluate SE of concrete with various conductive materials, which is mainly considered for new buildings. There is little research involved regarding both EMI shielding and the improvement of structural performance of existing structures. Hence, an increase in evaluation of concrete structures is required not only with respect to load resistance but to avoid "hard damage", as well as contribution to shielding effectiveness which will lead to a decrease in probability of "soft damage".

Concrete is the most commonly used construction material, this is due to its low construction cost and durability characteristics. Furthermore, concrete produces a certain efficiency in EMI shielding, it can be comparable to metal panels, with respect to their capacity as shielding materials after few modifications. The space of reinforced metallic rebar in the cement composites were considered at first. Hence, the impact and EMI resistant properties influenced by spacing of reinforced metallic rebar should explicitly defined and include SE properties after damage. A more recent material applied for both repair and strengthening of reinforced concrete structures is high-performance fiber reinforced composites (HPFRC), however, little information surrounding its SE exists [5, 6]. Therefore, strengthening of concrete structures will become very important not only for existing concrete structures, but also for strengthening of new concrete structural members so that they can withstand greater applied forces during service.

For above reasons, some researchers [3, 5, 6, 19–22] evaluated the SE of a cementitious composite structure strengthened by metallic grid. Most research was evaluated by prediction models (or numerical analysis) [19–22] which considered SE properties of metallic grid spacing and layer numbers. Some researcher [6] evaluated SE and impact resistance of a reinforced cementitious composites specimens, which were considered metallic grid hybrid with steel rebar. There was evaluation of the pure SE and impact resistance properties of cementitious composites specimens strengthened by metallic grid. Unfortunately, there is still a lack of data for cementitious composites strengthening and hybrid strengthening (hybrid using cementitious composites and metallic grid) in relation to the SE and external loading resistance properties (such as the relationship between damaged areas and shielding effectiveness).

Therefore, the influence of metallic grid parameters and high strength high ductility concrete (HSDC) on shielding effectiveness with and without impact loading are studied in this research. That is, this study mainly focuses on the development of high-performance EMI shielding and exterior impact resistance strengthening methods, considering a metallic grid and cementitious materials as the important ingredients. The four types of metallic grids (5×5, 10×10, 25×25, and 50×50 mm) and one types of HSDC were considered for surface strengthening in this study. First, a concrete wall with different types of metallic grids (5, 10, 25, 50 mm), and strengthening thickness of HSDC (5, 10, 20 mm) were considered to evaluate EMI SE, impact resistance, and SE after damage. Furthermore, the hybrid strengthening method is also considered in this study. The properties of all test specimen were fabricated under single and double strengthening state. Hence, this study aims to contribute basic data to the SE and impact resistance of concrete under metallic grid and/or cementitious composites strengthening.

2 Experimental program

Experimental evaluations comprising of EMI SE tests, drop-weight impact tests, and SE test after damage were conducted for small specimens. The experimental tests for small specimens were carried out to determine the high-performance EMI shielding and exterior impact resistance strengthening method. These data were helpful not only during design of the hybrid strengthening method of the middle-size specimens, but also the small specimen behavior gave a clear idea of the likely resistance improvement of the specimens under SE and/or impact testing. The prepared test specimens were tested after curing for 28 days.

2.1 Specimen preparation

Twenty-eight specimens were prepared using normal concrete with a compressive strength of 45 MPa at 28 days. The concrete specimens were strengthened with single- and double-layer metallic grids and HDSC as shown in Fig. 1. Square specimens with a length of 300 mm, width of 300 mm, and thicknesses of 100, 200, and 300 mm were evaluated for EMI SE according to the thickness, and specimens with thickness of 100 mm were evaluated for drop-weight impact test. Thus, compared with SE before and after damage by impact load. The manufacturing of molds, metallic grid setting, concrete mixing and casting works were all carried out in one concrete company to ensure quality control.

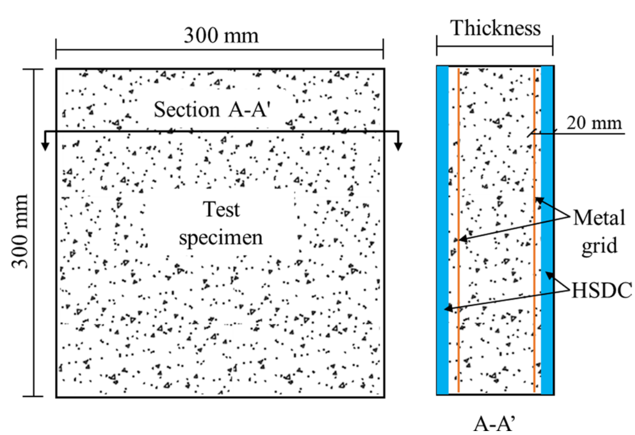

Fig. 1 Details of the test specimen

2.2 Materials properties

The test specimens were fabricated from normal concrete (NC, $f_{ck,28}$ of 45 MPa), which consist of water, type I Portland cement (corresponds to the ASTM C150 [23]), crushed fine and coarse aggregate (a maximum size of 18 mm), as shown in Table 1. Two different types of strengthening material have been measured by the SE and impact resistance in this study. The details of HSDC and metallic grid are presented in Tables 2 and 3, respectively. The constituent materials adopted to prepare the HSDC used in this study contained type I Portland cement, silica fume (a specific surface area of 200,000 cm^2/g and density 2.20 g/cm^3), filler (a specific surface area of 2.65 cm^2/g and density 0.75 g/cm^3), silica sand (a diameter ranging from 0.08 to 0.30 mm), 1.5 vol.% of hybrid fiber (1.0 vol.% of high strength straight fiber and 0.5 vol.% of high strength polyethylene fiber), and superplasticizer was adopted. The material properties have been already published in previous research (compressive strength [24], flexural strength [24], direct tensile strength [24, 25], splitting tensile strength [24, 26], in which the deviation between this study and previous research values are smaller than 3 MPa. The results values are described in Table 4.

2.3 Strengthening schemes

The strengthening plan for the test specimens are shown in Table 5. For convenience in producing the metallic grid system over the concrete specimens, the specimens were casted in five steps. First, 20 mm thickness of concrete was casted in the mold. Second, laid the metallic grid flat and end fixed with mold. Third, casted the concrete until it was 20 mm from the top. Fourth, laid the metallic grid as described in the second step. Fifth, casted concrete and surface finishing.

For the test specimens strengthened by HSDC system. The thickness of NC specimen was casted less than aiming (considered strengthening thickness and except it). Then, two sides of the NC specimen surface was processed to a certain degree of roughness, which was achieved through the use of surface chiseling (electronic breaker) in this study. This surface treatment method can achieve high roughness and bond properties with strengthening materials [26]. Two side surfaces of NC specimen were cleaned of any extra dust or particles after surface treatment, then HSDC was cast to complete the strengthening every other day. All specimens were cured in a room at a temperature of 20 ± 1 °C and humidity of 60 ± 5% for a 28-day period.

Table 1 Mixture proportions (by weight)

w/c	Water	Cement	Fine aggregate	Coarse aggregate	SP
0.43	0.43	1.00	2.15	2.42	0.8%

Table 2 Mixture proportion of HSDC

	w/b	Water	Cement	Silica fume	Silica filler	Silica sand	Steel fiber	Polyethylene fiber	SP
HSDC	0.172	0.215	1.00	0.25	0.30	1.10	1.0%	0.5%	3.0%

NSHSDC high-strength high-ductility concrete, *w/b* = water to binder ratio, *SP* superplasticizer

Table 3 Properties of metallic grid

	G5	G10	G25	G50
		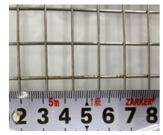	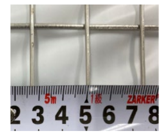	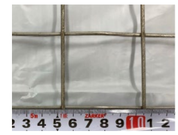
Diameter (mm)	0.73	1.18	1.90	2.38
Tensile strength (MPa)	987/1013	836/821	842/866	797/806

Table 4 Strength test results (28-day)

	Compressive strength (MPa/CV)	Flexural strength (MPa/CV)	Tensile strength (MPa/CV)	Remarks
NC	44.6/0.2	25.7/0.4	3.9/0.5	Splitting tensile strength test
HSDC	122.3/0.1	22.9/6.5	9.7/1.6	Direct tensile strength

CV coefficient of variation

Therefore, the following nomenclature is adopted to distinguish between test specimens. For example, T1-M5-S, where the first item T1 denoted 100 mm thickness of test specimens; the second item denoted strengthening materials (such as, M5 denoted 5 mm metallic grid); third item S denoted single side strengthening method (for test specimen strengthened by HSDC, H5-S denoted 5 mm single strengthened using HSDC); details shown in Fig. 2.

2.4 Electromagnetic interference shielding test

Currently, there are many different SE test standards and specification for various materials. The measuring instrumentation test methods include, flange coaxial method, coaxial transmission line test method, IEE Std 299 test method, MIL-STD-285 test method, and improved MIL-STD-285 test methods and so on. However, there are obvious disadvantages in these test methods, given test specimens are typically too large, difficult to manufacture, hardly fixed to test specimen, and low measurement repeatability [3, 5, 27, 28]. Considering these problems, the near-field condition test method using small size test specimen was used for concrete specimen, which utilized an EMI device with a frequency range of 300 to 1500 MHz for the transmitting and receiving facility [6, 29, 30]. This acknowledged EMI shielding test result proved similar behavior to the test based on MIL-STD-285. The test setup and details are shown in Fig. 3. For this instrumentation, the calibrations were achieved to ensure correct measurement from the nominal value on the receiver before the test. The test specimen was placed between the transmitting antenna and receiving antenna to complete measurement. The EMI shielding test was repeated six times for each test specimen, and the average values were used in this study.

2.5 Low velocity impact test

The impact test was conducted with a user-defined setup specifically made for such experiments as shown in Fig. 4. The specimen was bolted to the C shape steel support on all four sides, to provide a high support condition and prevent rebounding upon impact. The purpose of this study was to investigate the effects of EMI SE, and the damage (crack or scabbing) effects of specimen on the opposite face, and wherever possible reduce influence of the effective section reduction of specimen on the impacted face (spalling). The drop-weight with flat head caused little severe concrete damage of specimens at the impact face compared to hemispherical and curved heads [31], and the most severe damages at the negative bending moment zone [32, 33]. Therefore, to prevent severe specimen damage at the impact surface, the cylinder frustum (flat impact zone) drop-weight head is considered in this study. The specimen were subjected to drop-weight impact loading at their centers applying a

Table 5 Details of specimens

			Thickness (mm)	5 mm Grid	10 mm Grid	10 mm Grid	10 mm Grid	HSDC	
1	Type I	T1-M5-S	100	Single	–	–	–	–	–
2		T1-M5-D	100	Double	–	–	–	–	–
3		T3-M5-S	300	Single	–	–	–	–	–
4		T3-M5-D	300	Double	–	–	–	–	–
5		T1-M10-S	100	–	Single	–	–	–	–
6		T1-M10-D	100	–	Double	–	–	–	–
7		T3-M10-S	300	–	Single	–	–	–	–
8		T3-M10-D	300	–	Double	–	–	–	–
9		T1-M25-S	100	–	–	Single	–	–	–
10		T1-M25-D	100	–	–	Double	–	–	–
11		T3-M25-S	300	–	–	Single	–	–	–
12		T3-M25-D	300	–	–	Double	–	–	–
13		T1-M50-S	100	–	–	–	Single	–	–
14		T1-M50-D	100	–	–	–	Double	–	–
15		T3-M50-S	300	–	–	–	Single	–	–
16		T3-M50-D	300	–	–	–	Double	–	–
17	Type II	HD100	100	–	–	–	–	–	–
18		HD200	200	–	–	–	–	–	–
19		T1-H5-S	100					5 mm	Single
20		T1-H5-D	100					5 mm	Double
21		T1-H10-S	100					10 mm	Single
22		T1-H10-D	100					10 mm	Double
23		T1-H20-S	100					20 mm	Single
24		T1-H20-D	100					20 mm	Double
25		T2-H20-S	200					20 mm	Single
26		T2-H20-D	200					20 mm	Double
27		T3-H20-S	300					20 mm	Single
28		T3-H20-D	300					20 mm	Double

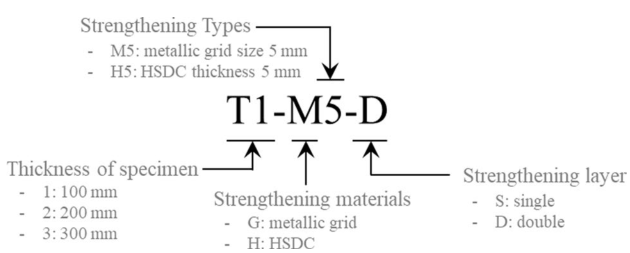

Fig. 2 Designation of test specimen

100 kg cylinder frustum headed metallic tup (a diameter of 70 mm) released from a height of 200 mm and increased at each loading step by 100 mm increment. A setup including a hydraulic system and a hook attached to the crane was used to release the drop tup by switching the height and releasing time. The dynamic response of the test specimens to the drop-weight impact load was measured using two types of sensory data. Vertical deflection of the specimen was measuring using laser type LVDT (KL4-120NV), which were placed at the central point of the bottom face of the specimen. Two load cells were set on either side of an invisible central axis support to measure the reaction force.

3 Results and discussion

3.1 Shielding effectiveness of specimen strengthened by metallic grid

3.1.1 Shielding effect of specimen reinforcement

The EMI SE of specimens with different metallic grid types are displayed in Fig. 5. The SE is the combination of reflection loss and absorption of the test specimens. Figure 5 shows two specimens of different thicknesses (100 and 300 mm) strengthened with and without metallic grid. A traditional method is to simply increase thickness to increase EMI SE and is widely used in construction. The increase in specimen thickness effectively results in an increase in SE,

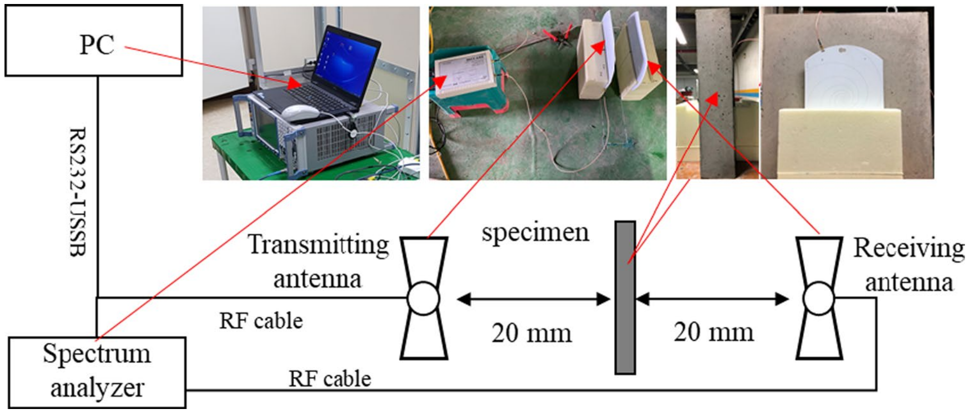

Fig. 3 Shielding effectiveness test setup

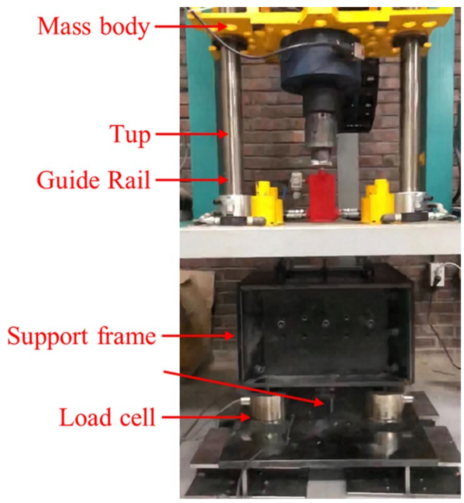

Fig. 4 Details of the drop weight impact test

which does not increase linearly. This is a result of increasing thickness of concrete leading to an increase in reflection loss and absorption [5, 6, 28]. As with most research, concrete thickness mainly influences the frequency, resulting in SE increasing due to frequency as and concrete thickness increase. The specimen strengthened with metallic grid displayed an increase in SE with a decrease in grid size, which were 0.2–7.9, 1.4–20.9, 4.0–22.7, and 8.2–31.3 dB, respectively, higher than specimens without a metallic grid. The specimens reinforced by different types of metallic grids were improved to a certain extent in SE, with the smaller the grid size, the more evident the SE no matter single- or double-layer reinforcement. This is a result of the metallic grid deadening the penetration, owing to the continuous electrical pathway, and metallic grids exhibit a reflection interface that attenuates the transmission wave in the concrete matrix [3, 34]. There are, of course, the specimen strengthened by two layers which exhibit more SE than those of single layer. This is because double-layer metallic grid reinforcement exhibits dual function of reflection interface and small metal waveguides. Nevertheless, SE of specimens strengthened by a double layer is significantly smaller than the sum of two single layer types. This is due to electromagnetic waves penetrating the first metallic grid layer which exhibited numerous reflections in the two metallic grid spaces, and after that, there were still some waves penetrating the second metallic layer, thus causing a decrease in the total SE of metallic grid reinforcement specimen [3, 34–36]. This phenomena is hardly found in the specimens strengthened by 50 mm metallic grid as mentioned in previous research [5, 6]. Therefore, from the simple SE point of view, there is blindly to be able to increase strengthening metallic grid layers cannot effectively improve the SE. This also indicates that researchers must consider many factors synthetically and all kinds of disadvantageous factors, so that it is possible to obtain greater SE. For all these reasons, using two metallic grid layers was found to be better than a single layer, but significantly affected by spacing of metallic grid layers. Thus, the negative resonance will exhibit if the set interlayer spacing is improper [36, 37]. Furthermore, The SE of specimens with different variations of (size and layer) metallic grids exhibit crests and troughs in different frequencies, which was caused by resonance at that frequency. Resonant frequency [35] can be simply calculated using $f_{mnl} = 1/\left(2d\sqrt{\mu\varepsilon}\right)$. Where μ is magnetic permeability of concrete (nonmagnetic materials), ε is permittivity of free space.

3.1.2 Shielding effect of specimen reinforced by different types of metallic grid

Figure 6 shows the shielding effect of the inclusion of different types of strengthening metallic grids within the specimens. This figure shows that a decrease in metallic grid size led to an increase SE. This can be explained by the fact that denser metallic grids lead to an increase in metal shielding layer surface area and stronger reflection. There are also researchers [5, 34, 38] that state decreasing metallic grid spacing corresponds to a smaller penetration channel and thus, EMI field penetration and high SE. Hence, the

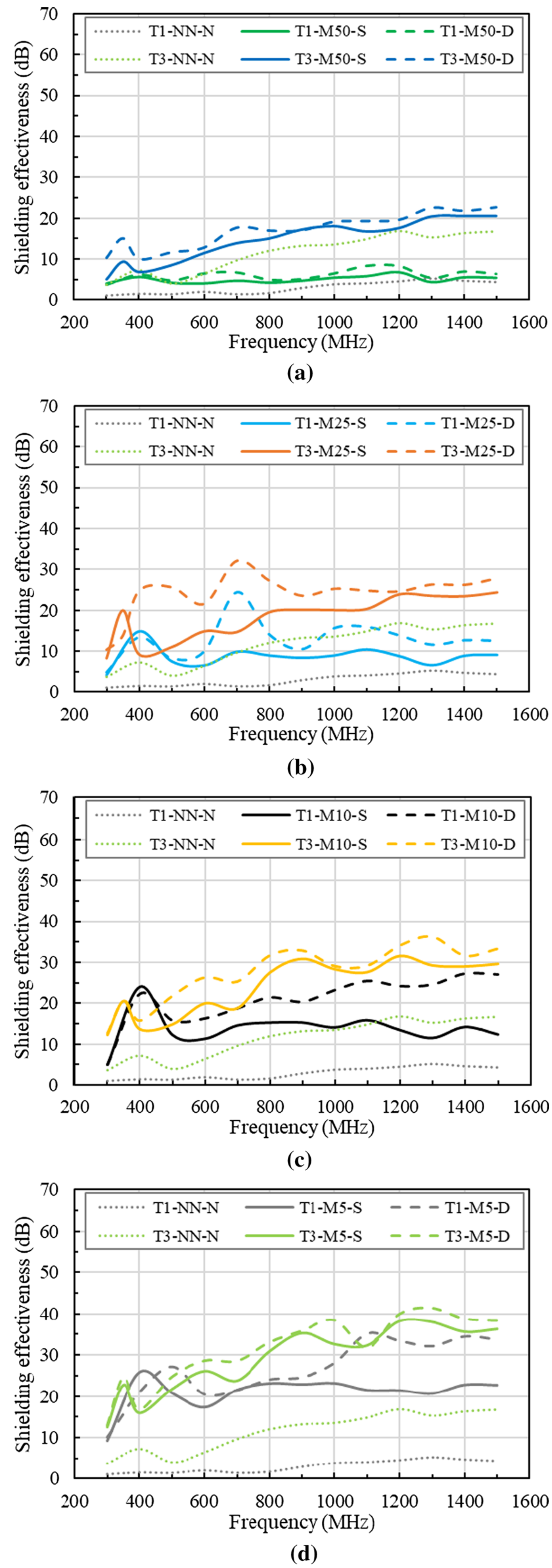

Fig. 5 Shielding effectiveness of specimens strengthened by metallic grid: **a** specimens strengthened by M50, **b** specimens strengthened by M25, **c** specimens strengthened by M10, **d** specimens strengthened by M5

specimen strengthened by 5 mm metallic grid (T1-M5-S, T1-M5-D, T3-M5-S, T3-M5-D) shows the greatest SE compared with others in the test frequency. It also indirectly proves that the same spacing of reinforcement rebars with a bigger diameter helped to improve the EMI SE, which is consistent with the results of previews research [5, 6, 19]. There is an interesting phenomenon that neither specimen strengthened single layer, double layers, smaller metallic grid type, nor increase thickness ($\leq$300 mm) of specimen hardly over the 40 dB in the SE properties. That would mean using metallic grids to improve SE has a limit, as every metallic grid can only take small metal waveguides and its cutoff wavelength is approximately 2 times of grid hole size [37]. This is also due to electromagnetic waves penetrating the first metallic grid layer, exhibiting numerous reflections in the two metallic grid spaces, and after that, there were still some waves penetrating the second metallic layer.

For the metallic grid strengthening specimen or reinforced concrete, many researchers [6, 27] have tried to simply define the relationship between free area ratio of grid (mesh) and EMI shielding effectiveness. The free space (that the electromagnetic wave can penetrate) to total strengthening grid area ratio can be defined as the free space area ratio, which can be established through a relationship with the shielding capacity. Figure 7 shows the metallic grid variation relationship with the SE which exhibited an exponential behavior. From this figure, the specimen strengthened by two layers exhibited more SE than those of single layer. The results obtained in this research are equivalent and even superior for the sparse grids tested, when compared with shielding values found in the literature [6, 27, 34]. For the single metallic grid strengthening, the free space area ratio smaller than 160% produced an SE that was over 20 dB. For the double-layer specimens with a free space area ratio smaller than 300% exhibited a SE that was over 20 dB, and a free space area ratio smaller than 140% produced a SE that was over 30 dB. This result proved again the phenomena and slightly modified that. Furthermore, double-layer metallic grid strengthening can occur as SE was more 40 dB, which the free space area ratio was smaller than 100%, similarly with the hybrid metallic mesh strengthening of previews research [6]. However, the free space area ratio should be smaller than 55% for single metallic grid strengthening. This research indicates that concrete elements with metallic grids were more useful compared to those that only increased thickness, whereas compared to both the double-layer strengthening method was more efficient. Furthermore, specimens strengthened by 50 mm metallic

Fig. 6 Comparison of shielding effectiveness of different metallic grid: **a** 100 mm thickness specimen with single layer, **b** 100 mm thickness specimen with double layers, **c** 300 mm thickness specimen with single layer, **d** 300 mm thickness specimen with double layers

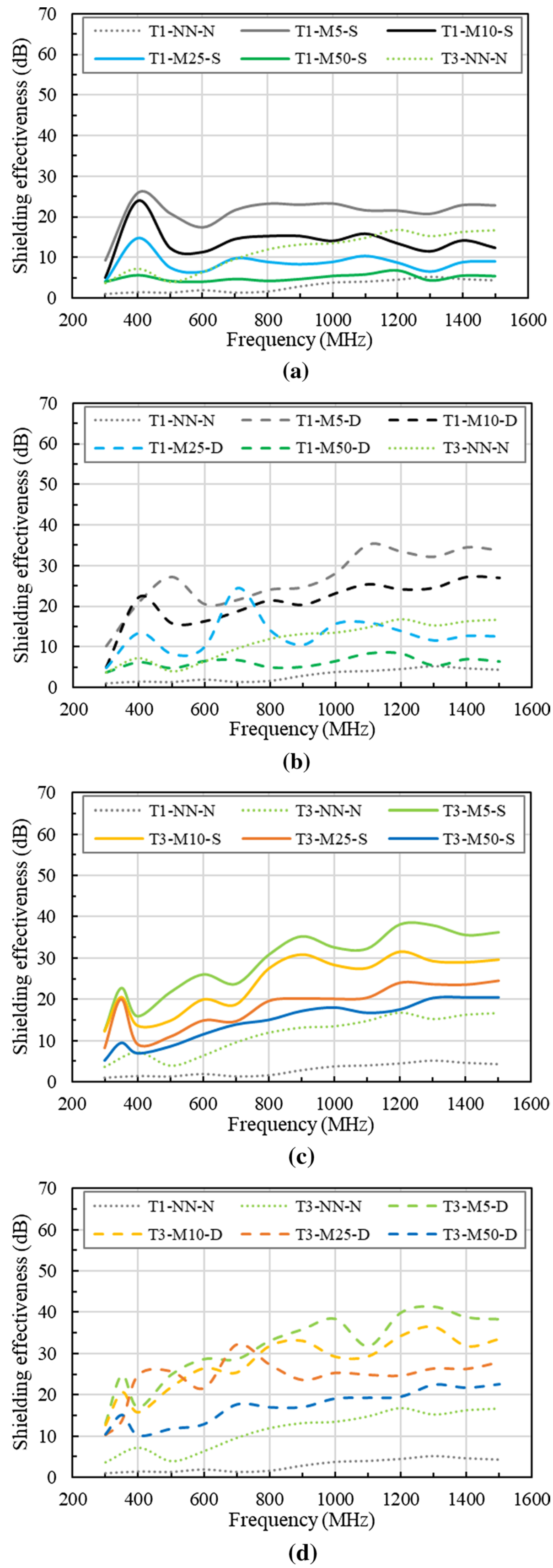

grids with single- or double-layers exhibited similar SE values, which were approximately 5.6 and 6.9 dB, respectively (Fig. 5a). This is because the grid holes were parallel and in lie with each other across both layers in the specimen, thus almost negligible as the reflection interface attenuates the transmission wave in the concrete matrix. It has been indirectly demonstrated that non-parallel setup of the two layers in the specimen can further improve SE compare do parallel configurations. This is also coherent with the results of literature [5, 6, 20], which shows concrete reinforced with over 50 mm of rebar spacing did not improve SE. Therefore, this research is simply provided to contribute basic data of shielding design, making it possible to design in advance a wall element whose shielding performance is customized to specific needs.

3.2 Shielding effectiveness of specimen strengthened by HSDC

HSDC containing hybrid steel and polyethylene fibers (randomly oriented) were developed and investigated, hybrid fibers are well known for their ability to reduce cracking, improve toughness, tensile strain and enhance electrical conductivity [6, 24, 25]. However, HSDC and strengthened for EMI SE still need further insights. Figure 8 shows the results of the EMI SE test for HSDC with different thicknesses, compared with two types of steel fiber reinforced concrete (test results referred from Yuan et. al 2021). The specimens reinforced with 0.75 and 1.50 vol.% content of steel fibers show similar EMI SE behavior, which 0.75 vol.% of steel fibers was sufficiently over the percolation threshold [5, 6]. Steel fibers when randomly dispersed in the concrete matrix produce a conductive grid, which is an effective continuous electrical pathway that increases the EMI SE [2, 5, 6]. Thus, the SE of steel fiber reinforced concrete specimens were almost 40 dB and 50 dB from 500 to 1500 MHz, respectively, except influence of resonance. The HSDC specimens with 100, and 200 mm continues to increase SE properties at 300 to 1000 MHz, and the SE of specimens were almost 40 dB and 50 dB from 1000 to 1500 MHz, respectively. It can be interpreted that SE of HSDC was lower than fiber reinforced concretes (F0.75-N, and F1.50-N), even though fiber contents of HSDC was higher than F0.75-N specimens. Influenced mainly by the fiber length of HSDC (l_f = 19.5 mm) which is significantly short than fiber reinforced concrete (l_f = 35 mm). The shape and size of the fibers, fiber length, the aspect ratio of factors played important roles in the SE of the fiber reinforced concrete [27].

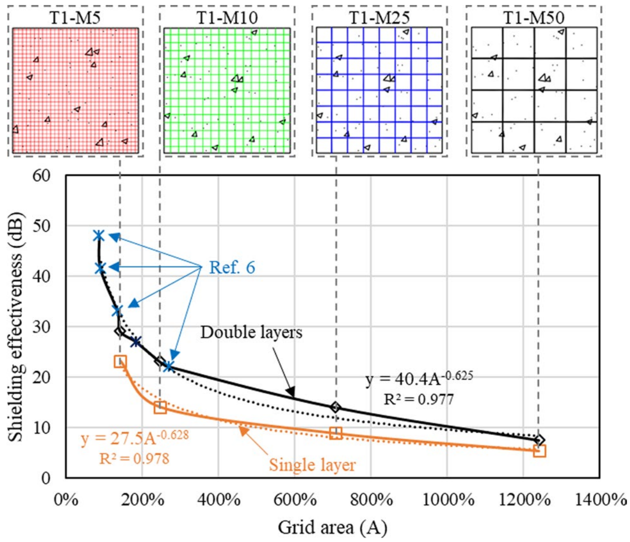

Fig. 7 Comparison of shielding effectiveness of variation of the free space area ratios

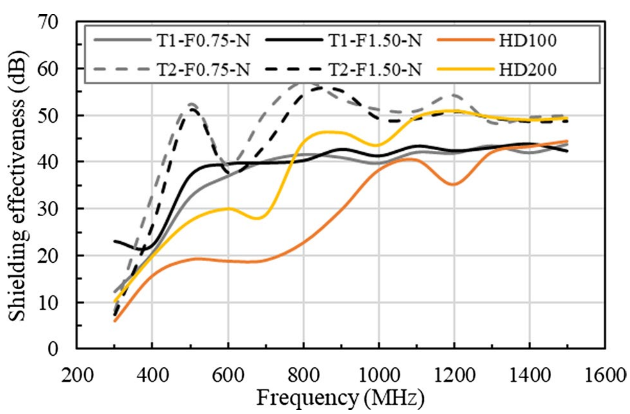

Fig. 8 Comparison of shielding effectiveness of variation of the fiber reinforced concrete

Figure 9 shows the results of the EMI SE test for concrete strengthened by different thickness of HSDC. As the strengthening layer thickness increased in specimen with the same initial thickness, the SE not only increased at the same test frequency but also improved as the frequency was increased as shown in Fig. 10a. Specimens strengthened with 5 mm one-layer HSDC exhibited greater SE compared to 200 mm thick concrete specimens without any strengthening and similar with 300 mm thick specimens. In particular, the SE noticeably increased when using double-layers HSDC strengthening, similarly to results seen when using double-layer metallic grid reinforcement (Fig. 10b). However, with increasing HSDC thickness, negative resonance peaks shift toward the lower test frequencies. This can be explained by the cancellation of reflected waves of the first and second HSDC layers at the matrix of the absorber materials, this occurred when the distance of two strengthened layers had approximately a quarter of the propagating wavelength multiplied by an odd number (thickness = (odd number x propagating wavelength in materials)/4) [2, 35]. However, the SE of specimens with different thickness strengthened by same HSDC conditions were similar for the entire test frequency range (Fig. 9c and d).

Furthermore, according to the influence of the spacing of two strengthening layers in the HSDC strengthened specimen, the acquisition of great SE for specimen strengthened by HSDC does not mean a simple addition of strengthening thickness problem, as shown in Fig. 10a. For the same total strengthening thickness, the double layer strengthening specimens were slightly higher than those of single types, which were approximately 1.5–9.1 dB during 600–1400 MHz. This demonstrates that thickness and spacing of HSDC is the key factor for the SE and there is the direct correlation between them. The SE properties of concrete specimens have an e-exponential function relationship with the strengthening thickness. To predict this e-exponential function shape curve of specimens, the simple prediction model for specimen strengthened by HSDC, in this research, was proposed as follows:

$$SE_{HSDC} = SE_{plain} + e^{\left(a(\ln(1+T))^{b}\right)}, \tag{1}$$

where SE_{plain} is the specimens without any strengthening, T is the strengthening thickness of HSDC, a and b are the regression coefficients.

The predicted values of specimens strengthened by single- or double-layers show good agreement with experimental results, in which the coefficient of determinations (R^2) are 0.989 and 0.994, respectively. The specimens strengthened by double layers are improved by 35.4–65.7% for SE properties compared to those of single layer types based on the prediction equation. It is interesting to observe that the EMI SE of specimens strengthened with HSDC containing single or double layers were mainly affected in 1000–15,000 MHz, and specimens strengthened with metallic grid were significantly affected in 300–1000 MHz (Figs. 6 and 10). It was verified that metallic grids mainly influence low frequency, and metallic fibers mainly influence high frequency [2, 5, 6]. Hence, the hybrid specimen using metallic grid and HSDC to strengthen the concrete specimens could significantly improve the SE.

3.3 Shielding effectiveness of specimen with hybrid strengthening

The specimens strengthened by 0.75 vol.% of hooked-end steel fiber, 5 mm metallic grid or HSDC exhibited great SE properties, thus, evaluation of the SE of specimens

Fig. 9 Comparison of shielding effectiveness of different HSDC: **a** 100 mm thickness of specimen with single layer, **b** 100 mm thickness of specimen with double layers, **c** different thickness of specimen with single layer, **d** different thickness of specimen with double layers

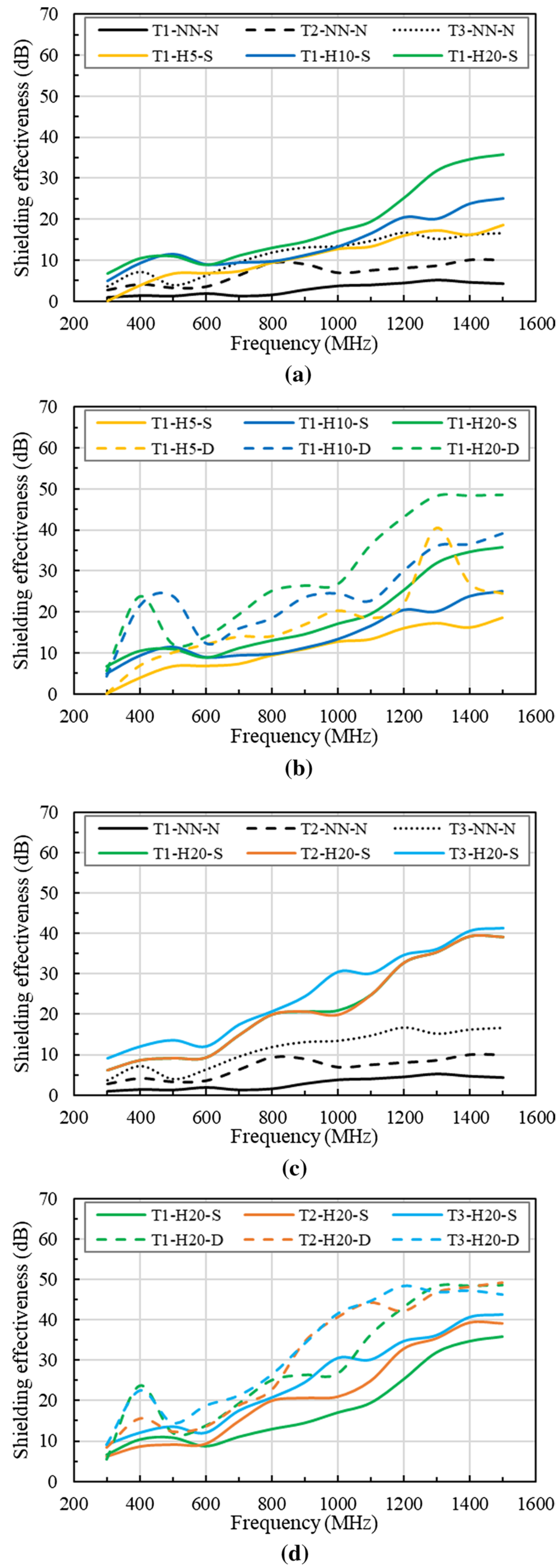

with hybrid strengthening materials is necessary. Hence, three types of hybrid specimens (dimensions of $300 \times 300 \times 300$ mm^3) were fabricated. The three different hybrid specimens were designed using a 50 mm metallic grid and 0.75 vol.% steel fibers, 5 mm and 50 mm metallic grids, and 5 mm metallic grid and HSDC. The EMI SE test configuration was set up based on MIL-STD-1881–125 Appendix A [39], which can evaluate in the frequency range of 600–2000 MHz. The details of configuration are already validated and used by many researchers [5, 21, 40].

Figure 11 shows the test results of the SE comparison for specimens with three types of hybrid strengthening combination. Among these test specimens, the specimens strengthened by hybrid double layer grids (T3-M50D-M5D) displayed the lowest SE and a decrease in SE with increasing test frequencies, which decrease from 74.39 dB at 600 MHz to 54.15 dB at 2000 MHz. It shows that the metallic grid used in concrete specimens mainly affect low frequency and effectively improve the SE properties. It is worth noting that specimen strengthened by 50 mm grid and 0.75 vol.% steel fibers, T3-M50D-F0.75, exhibited similar SE values at the test frequency, keeping the SE values in approximately 80 dB. This was presumably because the 0.75 vol.% of steel fibers formed an effective continuous electrical pathway in the matrix based on uniform distribution to improve the SE in the high-frequency region. According to the phenomena where the metallic grid (which are shown in T3-M50-M5D) exhibit similar SE values in the test frequency. However, the specimen T3-M50D-H20D exhibited a parabolic shape SE in the test frequency, and exhibited higher SE than other specimens. The maximum SE value 100 dB was exhibited at 1400 MHz. But the lowest SE value 60 dB was exhibited at a low frequency of 600 MHz. Therefore, it is suggested that the hybrid strengthening method used in concrete structures could be chosen according to the application aim of SE.

3.4 Shielding effectiveness of specimen after impact test

3.4.1 The results of low-velocity impact test

The number of drop blows versus with maximum reaction force, maximum deflection, crack numbers, and crack width are shown in Figs. 12 and 13. These results show the maximum reaction force recorded at each impact loading step. The reaction force is shown to abruptly decrease at a certain drop blow, which means specimen failure. Measuring

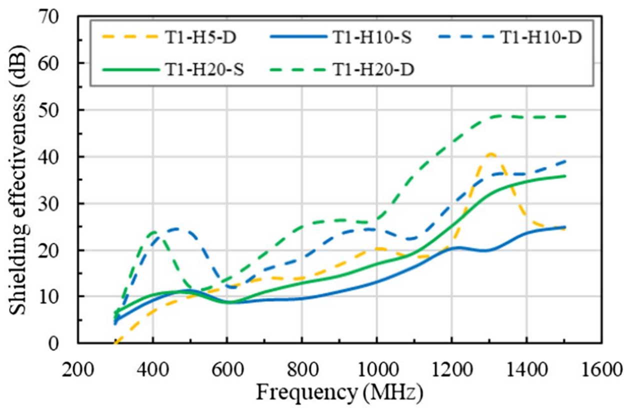

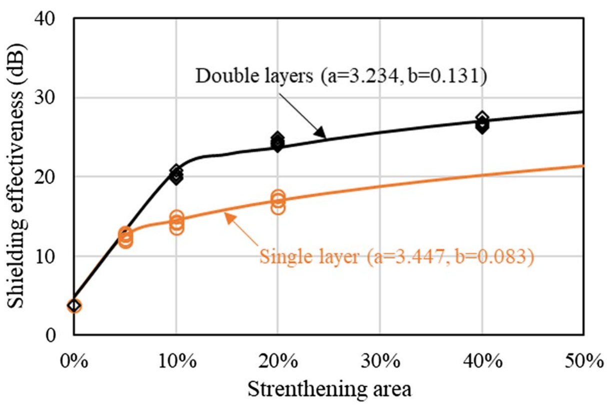

Fig. 10 Comparison of shielding effectiveness of different strengthening method: **a** shielding effectiveness of different combination strengthening, **b** comparison of shielding effectiveness of variation of strengthening area

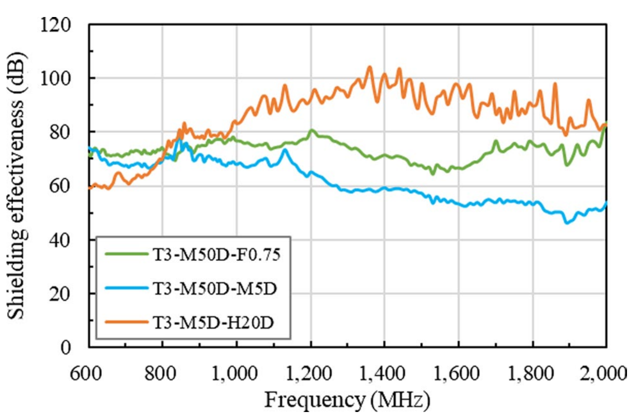

Fig. 11 Comparison of shielding effectiveness of different hybrid strengthening

number of drop blows to cause the maximum reaction force gave an indication of improvement in capacity of specimens subjected to impact load due to strengthening types.

The maximum reaction force and crack numbers exhibited which damage intensity has a reverse relationship with specimen strengthened by metallic grid size, as shown in Fig. 12. The specimen without any strengthening failed at the first drop weight, specimen strengthened by 5 mm or 10 mm failed at the fourth loading step, and specimens strengthened by 25 mm or 50 mm failed at the third loading step. Compared with the specimen without any strengthening, the specimens strengthened with grids exhibited a greater reaction force and many drop-blows, as a result these specimens were able to undergo greater reaction forces before failure, which were approximately 4.1–6.4 times higher than those of specimen without any strengthening. From comparison of magnitude and crack development at each loading step, it is concluded that specimens strengthened with smaller grid size decrease the development of concrete debris. However, in a manner similar to that of previous literature [22, 41–43], reducing the grid size in grid strengthened specimens had limited influence on the progression of midpoint displacement before failure. It is apparent from the near identical test result, no appreciable change in displacement was observed when the grid strengthening ratio was further decreased from 0.094 to 0.068%.

The crack orientation appearance on the bottom surface was that of a radioactive shape, with crack widths ranging from 0.05 to 0.08 mm; few visible cracks and limited scabbing were observed after the first drop blow. Succeeding drop weight loading led to diagonal fractures in the specimen, which stemmed from radioactive shape cracks developed under prior impacts (Fig. 14). Large diagonal cracks were evident on the bottom face of specimens and, despite this, the specimens sustained their integrity as the grids crossing the cracks prevented their opening. Furthermore, the failure mode from scabbing to large or pure diagonal cracks. The failure pattern of this test specimens indicated that the decrease in strengthening grid reduced crack width and the development, deflection, and magnitude of damage at the bottom surface of specimens as found in previous research [42, 43].

The reaction force and deflection of the specimens strengthened by HSDC was significantly influenced by the thickness of HSDC, as shown in Fig. 13. It can be seen that as the HSDC thickness increased so did the maximum reaction forces experienced, additionally the later step impacts tended to increase more gradually, H20-D in particular shows similar values with HD100 before the fourth impact. The total maximum reaction force of specimen H20-D exhibited 2.2 and 1.6 times higher values than those of H5-D and H10-D, respectively. It was interesting to observe that the specimen H5-D exhibited a similar reaction force compared with specimen M5-D. Furthermore, the specimens strengthened by 10 mm or more of HSDC external reinforcement show approximately 1.2–1.9 times the reaction

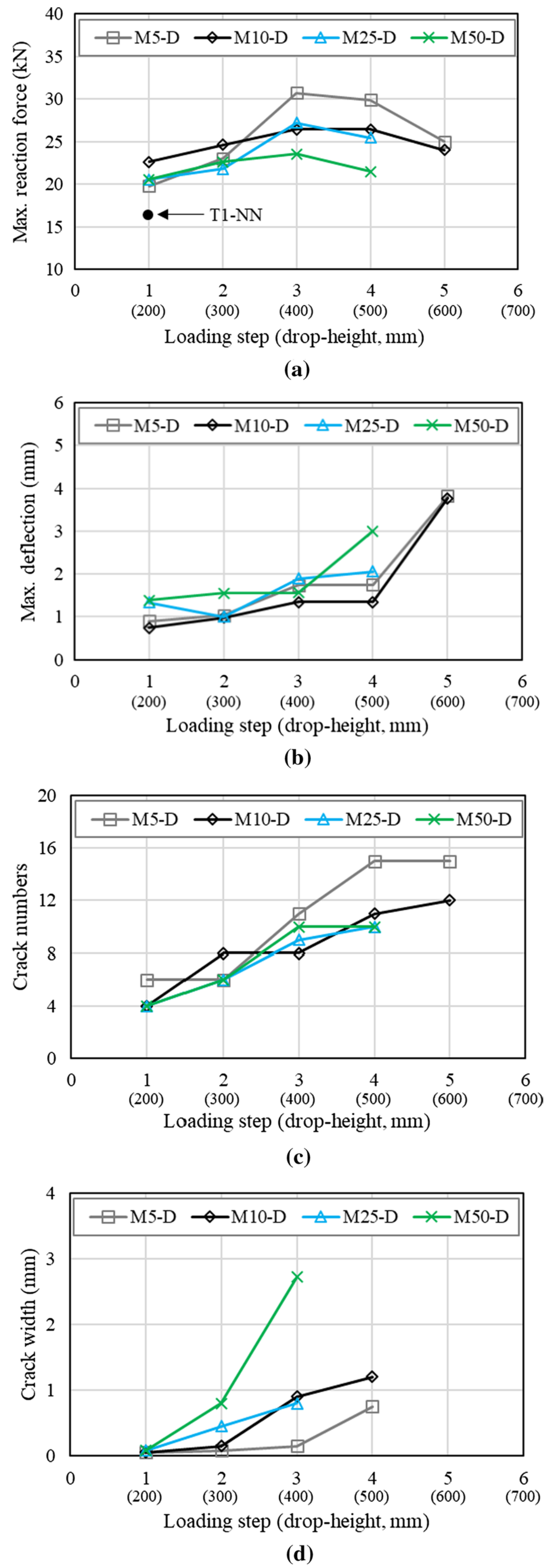

Fig. 12 Impact test result of specimens strengthened by metallic grid: **a** Max. reaction force at each loading step, **b** Max. deflection force at each loading step, **c** crack numbers at each loading step, **d** Max. crack width at each loading step

force seen from M5-D. And the addition of HSDC thickness reduced the maximum displacement, particularly for impact performed on H20-D.

Both radial and radioactive cracking were observed in the specimen under the first impact load; however, compared to the cracks developed in the specimens strengthened by metallic grid, the crack widths were similar, ranging from 0.05 to 0.15 m. Distinct diagonal fractures were not apparent until after the second impact load was performed on specimens strengthened by 5 mm and 20 mm HSDC (H5-D, H-10D). The crack width was approximately 5.00 mm after the fourth drop blow for H5-D, and 5.50 mm after the fifth drop blow for H10-D. Specimen H20-D, which contained the largest strengthening thickness, was most resistant to impact loading. The cracking pattern on the bottom surface of the specimen exhibited primarily hairline cracks (0.05 mm) after the first impact load. The maximum crack width of 0.70 and 1.10 mm were measured at the fourth and fifth impact load, respectively. However, unlike H5-D and H10-D specimens, the strengthening material HSDC was effective in controlling the crack growth. Fiber bridging in large diagonal cracks on the bottom surface of the specimen were exhibited under the sixth impact load, and wide diagonal cracks that developed from the midpoint toward the edge of the specimen were observed. The specimens also fracture by the large diagonal cracks as shown in Fig. 14.

Furthermore, the influence of the strengthening methods on impact capacities of specimens using total imparted energy are shown in Fig. 15. The failures were found to conduct the behavior of the specimens under prescribed impact loading protocol, decreased grid size was found to have limited influence on impact capacity compared with HSDC strengthening. This obviously indicates that thick HSDC and smaller grid size strengthening significantly improve the impact capacity.

3.4.2 Shielding effectiveness of the specimens after impact test

The shielding effectiveness of concrete specimen are mainly influenced by effective thickness variation which influenced by external loads or environment factors as found in previous research [6, 44]. Hence the SE property was evaluated for the specimens after impact test in this study, using SE decrease ratio versus damage area ratio (damage area ratio include crack and scabbing area ratios).

Specimen M50D exhibited the largest SE decrease ratio compared those of other specimens, which was exhibited

Fig. 13 Impact test result of specimens strengthened by HSDC: **a** ▸ Max. reaction force at each loading step, **b** Max. deflection force at each loading step, **c** crack numbers at each loading step, **d** Max. crack width at each loading step

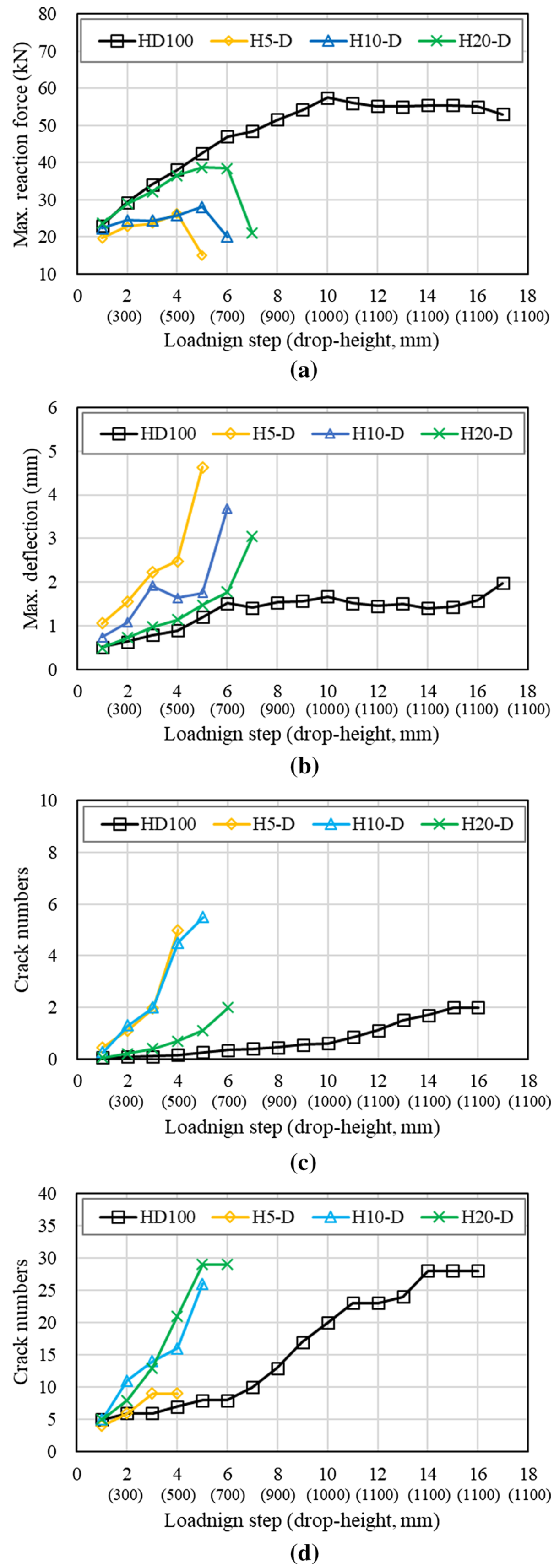

approximately as 30.8%. This is because spalling occurred on the center of the bottom surface at the impact region for the M50D specimen, which significantly reduced the effective thickness of the specimen. However, it is decreased accordantly with the specimen strengthened by decreasing metallic grid size. As found in above test results, the smaller grid mainly influenced the numbers of cracks developed and reduced scabbing of the bottom surface of the concrete specimen. Therefore, M5-D exhibited the smallest SE decrease ratio with a value of approximately 1.7% after impact test (damage area ratio was approximately 4.31%).

Figure 16a shows comparison of SE decrease ratio and damage area ratios of specimens strengthened by metallic grid. Similar research data of literature was combined and used in this to construct a logarithmical relationship which was simply established using the SE decreased ratio and damage area ratio. The R^2 value was slightly increased from 0.945 to 0.972 according to addition of more data from literature. It is once again proven that the damage area ratio will decrease by 5.84% and 26.95%, and at the SE decrease ratio by 20% and 30%, respectively. Furthermore, the SE decreased ratio of specimen strengthened by HSDC were also evaluated and shows in Fig. 16b. The specimens strengthened by smaller thicknesses of HSDC increased the SE decrease ratio. According to the uniformly distributed steel fiber, although multi-cracks occurred and reduced the effective thickness of specimen, the SE decrease ratio exhibited similar values in similar damage area ratios of specimens without different strengthening thickness.

4 Conclusions

This study evaluated the SE of concrete walls strengthened by metallic grids and high strength high ductility concrete. A variety of strengthening methods were used to evaluate the SE and impact resistance. From this investigation, the following conclusions can be drawn:

1) The specimen strengthened with metallic grids displayed an increase in SE with a decrease in grid size, which were 0.2–7.9, 1.4–20.9, 4.0–22.7, and 8.2–31.3 dB, respectively, higher than specimens without a metallic grid. Moreover, the specimens reinforced by different types of metallic grids were improved to a certain extent in SE, with smaller grid sizes producing more effective SE responses irrespective of single- or double-layer reinforcement.

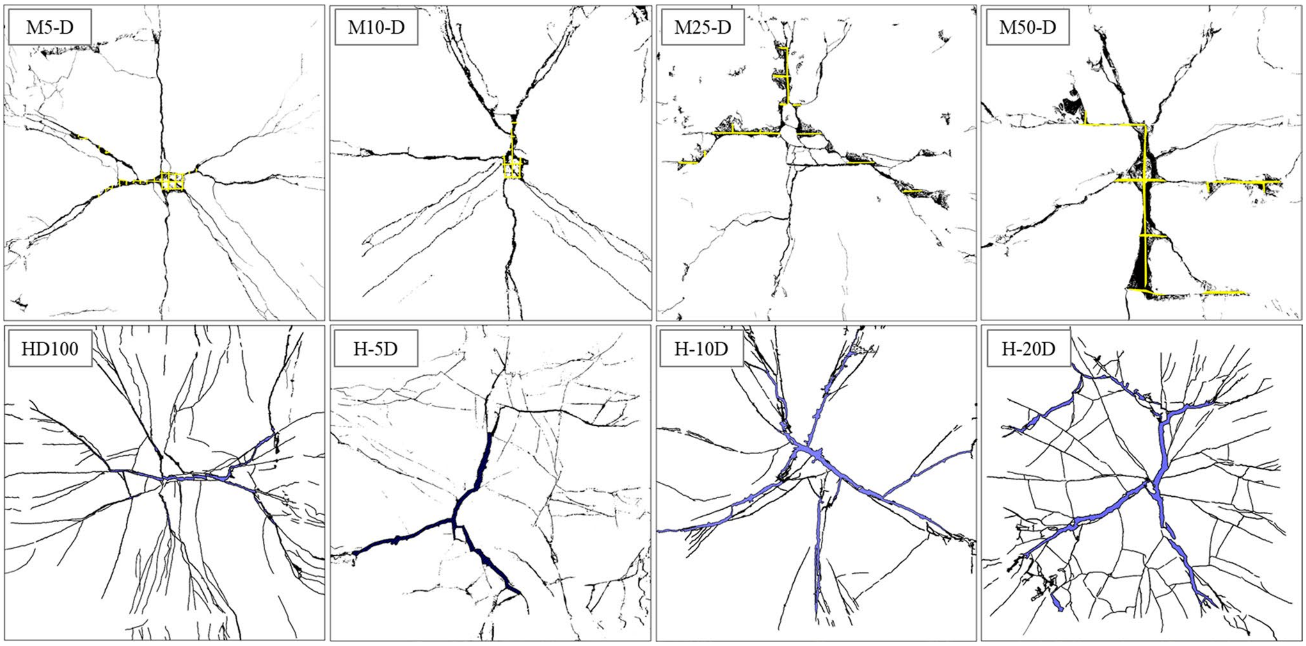

Fig. 14 Observed damaged after final impact

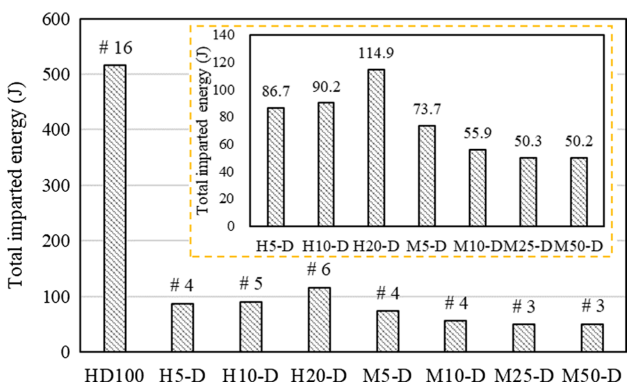

Fig. 15 Total imparted energy until failure

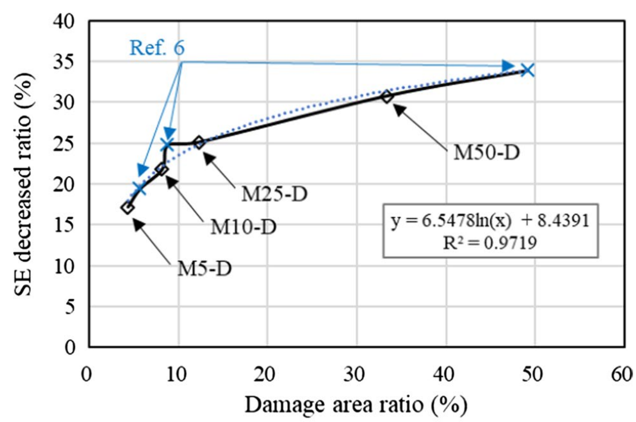

(a)

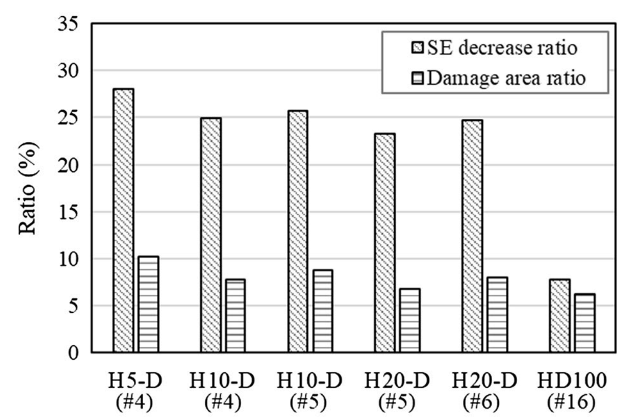

(b)

Fig. 16 Comparison of shielding effectiveness decreased ratio of variation of the damage area ratios: **a** specimens strengthened by metallic grid, **b** specimens strengthened by HSDC

2) For the single and double metallic grid strengthening, a free space area ratio smaller than 160% and 300% produced an SE that was over 20 dB, and a free space area ratio smaller than 140% creating an SE that was over 30 dB. Furthermore, specimens strengthened by 50 mm metallic grid with single-layer or double-layer reinforcement exhibited similar SE values, which were approximately 5.6 and 6.9 dB, respectively. It has been demonstrated indirectly that non-parallel setup of two layers in the specimen can largely improve the SE than those of parallel ones.
3) The SE noticeably increases from use of double-layer HSDC reinforcement, similarly in the case of double-layer metallic grids. However, with increasing HSDC thickness, negative resonance peaks shift toward the

lower test frequencies. The EMI SE of specimens strengthened with HSDC containing single or double layers were mainly affected in 1000–15,000 MHz, and specimens strengthened with metallic grid were significantly affected in 300–1000 MHz range. Hence, the hybrid use of metallic grid and HSDC to strengthen the concrete specimens could significantly improve the SE.

4) For the impact test results, the specimens strengthened with smaller metallic grid and thick HSDC showed significantly improved impact resistance, whereas the total imparted energy of G5-D and H20-D specimens appeared to be 31.9–46.7% and 27.4–32.5% higher than that of the other specimens, respectively. Based on the great impact resistance of hybrid reinforced specimens, the SE decreased ratio was significantly lower than those of other specimens.

Therefore, concrete structures that were strengthened by metallic grid and/or HSDC could be chosen according to the application aim of SE.

Acknowledgements This research was supported by a grant (19SCIP-B146646-02) from Construction Technology Research Project funded by the Ministry of Land, Infrastructure and Transport of Korea government.

Declarations

Conflict of interest There is no conflict of interest.

References

1. Guan H, Liu S, Duan Y, Cheng J. Cement based electromagnetic shielding and absorbing building materials. Cem Concr Compos. 2006;28:468–74.
2. Shukla V. Review of electromagnetic interference shielding materials fabricated by iron ingredients. Nanoscale Adv. 2019;2019(1):1640–71.
3. Choi JS, Yuan TF, Hong SH, Yoon YS. Evaluating of Electromagnetic shielding characteristics of reinforced concrete using reinforcing details. J Korean Soc Hazard Mitig. 2020;20(5):245–54.
4. Wanasinghe D, Aslani F, Ma GW, Habibi D. Advancements in electromagnetic interference shielding cementitious composites. Constr Build Mater. 2020;231:1–23.
5. Yuan TF, Choi JS, Kim SK, Yoon YS. Assessment of steel slag and steel fiber to control electromagnetic shielding in high-strength concrete. KSCE J Civ Eng. 2021;25:920–30.
6. Yuan TF, Choi JS, Hong SH, Yoon YS. Enhancing the electromagnetic shielding and impact resistance of a reinforced concrete wall for protective structures. Cem Concr Compos. 2021;122:104148.
7. Mazzoli A, Corinaldesi V, Donnini J, Di Perna C, Micheli D, Vricella A, Pastore R, Bastianelli L, Moglie F, Mariani Priminai V. Effect of graphene oxide and metallic fibers on the electromagnetic shielding effect of engineered cementitious composites. J Build Eng. 2018;18:33–9.
8. Li Y, Yu M, Yang P, Fu J. Enhanced microwave absorption property of Fe Nanopaticles encapsulated within reduced graphene oxide with different thicknesses. Ind Eng Chem Res. 2017;56:8872–9.
9. Jung MJ, Lee YS, Hong SG, Moon JY. Carbon nanotubes (CNTs) in ultra-high performance concrete (UHPC): dispersion, mechanical properties, and electromagnetic interference (EMI) shielding effectiveness (SE). Cem Concr Res. 2020;131:106017.
10. Bae H, Ahmad T, Rhee I, Chang Y, Jin S-U, Hong S. Carbon-coated iron oxide nanoparticles as contrast agents in magnetic resonance imaging. Nanoscale Res Lett. 2012;7(44):1–5.
11. Ozturk M, Akgol O, Sevim UK, Karaaslan M, Demirci M, Unal E. Experimental work on mechanical, electromagnetic and microwave shielding effectiveness properties of mortar containing electric arc furnace slag. Constr Build Mater. 2018;165:58–63.
12. Khalaf MA, Ban CC, Ramli M, Ahmed NM, Sern LH, Khaleel HA. Physicomechanical and gamma-ray shielding properties of high-strength heavyweight concrete containing steel furnace slag aggregate. J Build Eng. 2020;30:101306.
13. Tyagi G, Singhal A, Routroy S, Bhunia D, Lahoti M. A review on sustainable utilization of industrial wastes in radiation shielding concrete. Mater Today: Proc. 2020;32(4):746–51.
14. Mishra M, Singh AP, Gupta V, Chandra A. Tunable EMI shielding effectiveness using new exotic carbon: polymer composites. J Alloys Compd. 2016;688:399–403.
15. Yao WL, Xiong GX, Yang Y, Huang HQ, Zhou YF. Effect of silica fume and colloidal graphite additions on the EMI shielding effectiveness of nickel fiber cement based composites. Constr Build Mater. 2017;150:825–32.
16. Kamil Z, Tomasz P, Andrezej G. Influence of polymer modification on the microstructure of shielding concrete. Materials. 2020;13(3):498.
17. Xu H, Li Y, Han XS, Cai HZ, Gao F. Carbon black enhanced wood-plastic composites for high-performance electromagnetic interference shielding. Mater Lett. 2021;285:129077.
18. Yoon HN, Jang D, Lee HK, Nam IW. Influence of carbon fiber additions on the electromagnetic wave shielding characteristics of CNT-cement composites. Constr Build Mater. 2021;269:121238.
19. Zhou BH, Cheng G, Chen B, Chen ZM. Experimental investigation of EMP shielding effectiveness of reinforced-concrete cell model, CEEM’2000 (IEEE Cat. No.00EX402). 6703576 (2000) 296–300
20. Sneh A, Thakur P, Yadav K, Goyal R, Gupta M. An experimental analysis of EMI shielding effectiveness using multi layered metal meshed reinforced sustainable foam. J Eng Res Tech. 2020;9(2):662–5.
21. Jung MJ, Lee YS, Hong SG. Effect of incident area size on estimation of EMI shielding effectiveness for ultra-high-performance concrete with carbon nanotubes. IEEE Access. 2019;26(1):183105–17.
22. Yilmaz T, Kirac N, Anil Ö, Erdem T, Kacaran G. Experimental investigation of impact behavior of RC slab with different reinforcement ratios. Struct Eng. 2020;24(1):241–54.
23. ASTM C150, Standard Specification for Portland Cement, ASTM International, West Conshohocken, PA, 2007, pp. 1–8
24. Yuan TY, Lee JY, Min KH, Yoon YS. Experimental investigation on mechanical properties of hybrid steel and polyethylene fiber reinforced no-slump high-strength concrete. Int J Polym Sci. 2019;2019:4737384.
25. Yuan TF, Lee JY, Yoon YS. Enhancing the tensile capacity of no-slump high-strength high-ductility concrete. Cem Concr Compos. 2020;106:103458.
26. Yuan TF, Hong SH, Shin HO, Yoon YS. Bond strength and flexural capacity of normal concrete beams strengthened with no-slump high-strength, high-ductility concrete. Materials. 2020;13(19):4218.
27. Quintana S, de Blas JM, Pena J, Blanco J, Garcia LD, Pastor JM. Design and operation of a real-scale electromagnetic shielding

evaluation system for reinforced composite construction materials. J Mater Civ Eng. 2018;30(8):04018162.
28. Liu F, Lü X, Li YB, Yang J, Pan Z. Attenuation characteristics on high power microwave penetrating through reinforced concrete. Chin J Radio Sci. 2014;29(1):35–9.
29. Micheli D, Marchetti M, Pastore R, Vricella A, Gradoni G, Moglie F, Mariani Primiani V. Shielding effectiveness of carbon nanotube reinforced concrete composites by reverberation chamber measurements. In: International Conference on Electromagnetics in Advanced Applications (ICEAA), 2015, pp. 145–148
30. Micheli D, Pastore R, Vricelaa A, Delfini A, Marchetti M, Santoni F. Chapeter 9- electromagnetic characterization of masterials by vector network analyzer experimental setup, spectroscopic methods for nanomaterials characterization (Micro and Nano Technologies), 2017, pp. 195–236
31. Pham TM, Hao Y, Hao H. Sensitivity of impact behaviour of RC beams to contact stiffness. Int J Impact Eng. 2018;112:155–64.
32. Li HW, Chen WS, Hao H. Influence of drop weight geometry and interlayer on impact behavior of RC beams. Int J Impact Eng. 2019;131:222–37.
33. Kim YH, Choi JS, Yuan TF, Yoon YS. Building-information-modeling based approach to simulate strategic location of shelter in place and its strengthening method. Materials. 2021;14(13):3456.
34. Hyun SY, Kyoung JK, Lee HJ, Lee KW, Yook JG. Analysis of shielding effectiveness of reinforced concrete against high-altitude electromagnetic pulse. IEEE Tran Antennas Propag. 2014;56(6):1488–96.
35. Lu HD, Zhu F, Li X, Tang YT. Shielding effectiveness of reinforced concrete toward electric arcs in pantograph catenary systems of metro. Chin J Radio Sci. 2016;31(6):1209–15.
36. You BX, Deng WD, Li Y, Duan HQ. Influence of steel grid parameter on its shielding effectiveness for indoor distribution substation. J Shenzhen Inst Inform Tech. 2009;7(4):74–8.
37. Liu F, Lü X, Li YB, Yang J, Pan Z. Attenuation characteristics on high power microwave penetrating through reinforcement nets. High Power Laser and Part Beams. 2012;24(11):2713–7.
38. Giulio A, Antonio O, Stefano D. Shielding effects of reinforced concrete structures to electromagnetic fields due to GSM and UMTS systems. IEEE Trans Magn. 2003;39(3):1582–5.
39. MIL-STD-188-125-1, High-altitude electro-magnetic pulse (HEMP) protection for ground-based C4I facilities performing critical, time urgent missions. Department of Defense Interface Standard (2005)
40. Jang HJ, Song TS. Implementation of concrete block shielding effectiveness measurement system for RF shield. J Inst Electron Inf Commun Eng. 2018;55(12):85–91.
41. Sadraie H, Khaloo A, Soltani H. Dynamic performance of concrete slabs reinforced with steel and GFRP bars under impact loading. Eng Struct. 2019;191:62–81.
42. Hamid S, Alireza K, Hesam S. Dynamic performance of concrete slabs reinforced with steel and GFRP bars under impact loading. Eng Struct. 2019;191:62–81.
43. Trevor DH, Frank JV. Behavior of steel fiber-reinforced concrete slabs under impact load. ACI Struct J. 2014;111(5):1213–23.
44. Yoo DY, Kang MC, Choi HJ, Shin WS, Kim SH. Electromagnetic interference shielding of multi-cracked high-performance fiber-reinforced cement composites-Effects of matrix strength and carbon fiber. Constr Buil Mater. 2020;261:119949.